JOURNAL OF PROPULSION AND POWER
Vol. 17, No. 6, November–December 2001

Supersonic Combustion Experiments with a Cavity-Based Fuel Injector

Tarun Mathur*
Taitech, Inc., Beavercreek, Ohio 45430
Mark Gruber,† Kevin Jackson,‡ Jeff Donbar,§ Wayne Donaldson,§ and Thomas Jackson**
U.S. Air Force Research Laboratory, Wright–Patterson Air Force Base, Ohio 45433
and
Fred Billig††
Pyrodyne, Inc., New Market, Maryland 21774

Recent results from combustion experiments in a direct-connect supersonic combustor are presented. Successful ignition and sustained combustion of gaseous ethylene have been achieved using an injector/flameholder concept with low-angle, flush-wall fuel injection upstream of a wall cavity. Two interchangeable facility nozzles (Mach 1.8 and 2.2) were used to obtain combustor inlet flow properties that simulate flight conditions between Mach 4 and 6 at a dynamic pressure of 47.9 kPa. Mainstream combustion was achieved at equivalence ratios between 0.25 and 0.75 using only a spark plug and no other external ignition aids. Delta-force levels between 667 and 1779 N were measured, with corresponding combustor pressure ratios between 3.1 and 4.0. Video records of the flame zone show an intensely active combustion zone with rapid flame spreading. One-dimensional performance analysis of the test data indicates a combustion efficiency around 80% with an average combustor skin friction coefficient of 0.0028.

Nomenclature

C_f	=	skin-friction coefficient
H	=	nozzle exit height
L/D	=	cavity length-to-depth ratio
M	=	Mach number
P	=	pressure
Q	=	dynamic pressure
T	=	temperature
t	=	time
u	=	velocity
x	=	streamwise coordinate
y	=	transverse coordinate
ΔF	=	change in force
η_c	=	combustion efficiency
ϕ	=	fuel–air equivalence ratio

Subscripts

cb	=	combustor
cv	=	cavity
o	=	flight condition
t	=	stagnation condition
ve	=	vitiator exit station
4	=	combustor inlet station

Received 14 June 2000; revision received 13 June 2001; accepted for publication 24 June 2001. This material is declared a work of the U.S. Government and is not subject to copyright protection in the United States.

*Research Scientist; currently, Innovative Scientific Solutions, Inc., 2766 Indian Ripple Road, Dayton, OH 45440-3638. Member AIAA.

†Aerospace Engineer, AFRL/PRA, Building 18, 1950 Fifth Street. Senior Member AIAA.

‡Aerospace Engineer; currently, Jackson Design LLC, Beverly Hills, MI 48025.

§Aerospace Engineer, AFRL/PRA, Building 18, 1950 Fifth Street. Member AIAA.

**Deputy for Science, AFRL/PRA, Building 18, 1950 Fifth Street. Member AIAA.

††Consultant, 11280 Panorama Drive. Fellow AIAA.

Introduction

FUEL–AIR mixing, flameholding, pressure losses, and thermal loading are among the major issues that need to be resolved for the successful design and implementation of hydrocarbon-fueled supersonic combustion ramjet (scramjet) engines. A successful fuel-injection scheme must provide rapid mixing between the fuel and oxidizer streams, minimum total-pressure losses, and have no adverse effects on flameholding capability or thermal/structural integrity of the device. These requirements place somewhat conflicting constraints on the design of a viable fuel-injection scheme, and solutions to these problems are being actively sought internationally. A need exists for the development of a system that effectively integrates fuel injection and flameholding for supersonic combustion. Such a device would contribute significantly to the present research and industrial technology base.

Three recent publications have presented relatively comprehensive literature surveys on the subject of cavity flows and their relevance to flameholding in supersonic combustion engines.[1–3] Experimental and analytical research to date has predominantly examined the role of cavities in external flows (as wheel wells or bomb bays on supersonic aircraft),[4–24] although there have been studies examining their flameholding characteristics in low-speed[25–27] and high-speed flows.[1–3,28–38] Low-speed combustion studies with an axisymmetric cavity[26] found optimum flameholding performance using a cavity with its length-to-depth ratio L/D sized for the minimum aerodynamic drag. Longer cavities produced vortex shedding that resulted in unstable flames, and shorter cavities did not provide enough air entrainment to hold the flame. Experimental and numerical results were shown to agree closely on this point.[27] A study by Yu et al.[29] in an unheated Mach 2 flow, with fuel injection upstream of a variable L/D cavity, suggested that small-aspect-ratio cavities provide better flameholding capability than longer cavities with inclined aft ramp angles.

Combustion experiments with a cavity-based fuel injector/flameholder and gaseous hydrocarbon fuel are described in this paper. The baseline fuel injector/flameholder has low-angled fuel injection upstream of a wall cavity. This configuration represents a novel concept for injecting fuel and piloting a flame in a scramjet combustor in that all of the components are contained in the wall. In contrast to in-stream concepts that introduce additional friction drag, wave

drag, and cooling requirements to the combustor, this configuration uses no in-stream devices, thereby minimizing these detrimental effects and simplifying the overall combustor and system designs. Concurrent studies involving flush-wall injection upstream of similar cavities in nonreacting supersonic flow have provided valuable insights into the effects of cavity configuration (L/D ratio, offset ratio, aft ramp angle), fuel injection pressure, and imposed backpressure on drag, residence times, and fuel distribution within the cavity.[37,38] The combustion experiments described here, as well as some numerical simulations[36,39,40] of the cavity-based fuel injector/flameholder, have shown robust flameholding and combustion performance in a scramjet combustor simulating Mach 4–6 flight conditions at a dynamic pressure of 47.9 kPa.

Experimental Facility

The test cell receives continuous airflow of 13.6 kg/s at 5.17 MPa and a maximum temperature of 922 K with 20.7 kPa continuous exhaust from the Research Air Facility. Both liquid and gaseous fuel systems are available, including pumped JP-4, pressurized JP-7, ethylene, and hydrogen. Liquid- and gaseous-oxygen systems are available for make-up oxygen in the vitiated heater. A recirculated cooling-water system provides 158 l/s at 483 kPa; raw dump water at 2.4 MPa is also available. The entire flowpath is secured to a thrust stand for direct measurements of the thrust produced. This measurement may be combined with wall static pressure measurements and a performance analysis code to estimate the combustion efficiency. Additionally, the energy losses through the various water-cooled components, coupled with temperature measurements from a steam calorimeter, allow calculation of combustion efficiency.[41]

For the tests described here, Mach 1.8 and 2.2 facility nozzles were used with on-design flight Mach numbers near 3.5 and 4.5, respectively (see Table 1). However, due to the finite number of facility nozzles available, off-design tests were also performed with these nozzles by varying the stagnation temperature to achieve combustor inlet static temperatures (or velocities) corresponding to a range of off-design flight Mach numbers between 4 and 6. The increased range of flight Mach numbers simulated with these tests is associated with a corresponding compromise in combustor inlet Mach number and velocity (or static temperature).[42]

Hardware

Supply air enters a JP-4 fueled Marquardt Sudden Expansion vitiator capable of sustaining temperatures to 2500 K. The vitiator is fitted with a H_2/air igniter system. A water-cooled instrumentation section placed downstream of the vitiator permits stagnation temperature and/or pressure measurements with traversing probes, wall static pressure/gas sampling ports, and eight thermocouple ports in the inlet and outlet flanges. A water-cooled transition flange compresses the vitiated airflow from axisymmetric (254 mm i.d.) to two-dimensional (57.2 × 177.8 mm) as it enters the water-cooled facility nozzle. Two removable water-cooled isolator sections are positioned downstream of the nozzle. These sections are used to contain the precombustion pressure rise. A variable-geometry heat-sink combustor follows the isolator sections. This component has a flexible upper wall permitting combustor exit-to-inlet area ratios of up to four (configured with an area ratio of approximately 2.5 for tests described here). The combustor has removable inserts on all four walls allowing optical access, installation of instrumentation, and a wide parametric design space for fuel injection and flameholding concepts. Finally, a calorimeter instrumentation section housing water sprays, rakes, and probes connects the combustor to a steam calorimeter. An aerogrid (a metal plate with 1266 converging–diverging holes, providing approximately 85% area blockage) was placed in the calorimeter for some of the tests described here. The aerogrid was designed to homogenize any nonuniformities in the combustor exit flow before the flow encountered the thermocouples at the calorimeter exit. The calorimeter exit connects to an elbow through which the flow exits the test cell to an exhauster system. Figure 1 illustrates the internal flowpath of the rig from the entrance of the facility nozzle to the combustor exit.

The fuel injector/flameholder used for fuel injection and combustion experiments in the combustor has four low-angle (15-deg) fuel injectors (fed from a common manifold) across the span of the combustor, just upstream of a cavity-based flameholder. The cavity geometry can be varied by changing the L/D ratio, the distance downstream from the fuel injectors, and the aft ramp angle. For the experiments described here, the cavity aft ramp angle and L/D ratio were approximately 22 deg and 4.8, respectively. Ports are available in the bottom wall for fueling, ignition sources (for example, spark plugs), pressure taps, thermocouples, and gas sampling measurements. The baseline cavity geometry used in the present investigation is shown in Fig. 2. For experiments with the Mach 1.8 facility nozzle, the cavity was fueled from its bottom wall, through five spanwise ports located just upstream of the aft ramp; the cavity was not independently fueled for tests with the Mach 2.2 facility nozzle. Furthermore, to improve fuel penetration with the Mach 2.2 facility nozzle, the area of the main injector holes was reduced by approximately 50% relative to the size used with the Mach 1.8 facility nozzle.

Table 1 Simulation conditions

M_o	Q_o, kPa	M_4	T_4, K	P_4, kPa	u_4, m/s
3.5	47.9	1.74	468	64.6	753
3.5	95.8	1.74	468	132.4	753
4.0	47.9	1.96	523	66.3	892
4.0	95.8	1.96	519	126.8	888
4.5	47.9	2.17	577	67.0	1036
4.5	95.8	2.17	568	136.8	1029
5.0	47.9	2.39	628	66.7	1185
5.0	95.8	2.39	616	134.9	1173
5.5	47.9	2.59	679	66.4	1335
5.5	95.8	2.59	666	134.3	1322
6.0	47.9	2.79	730	65.7	1487
6.0	95.8	2.79	715	133.4	1472

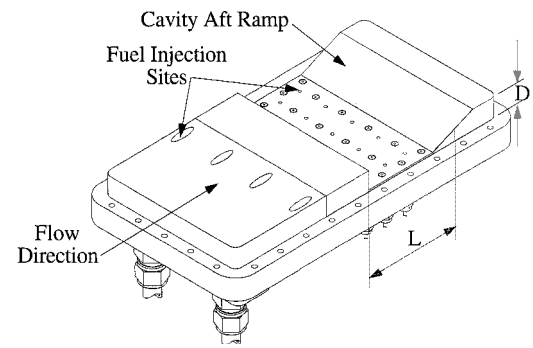

Fig. 2 Fuel injector/flameholder schematic.

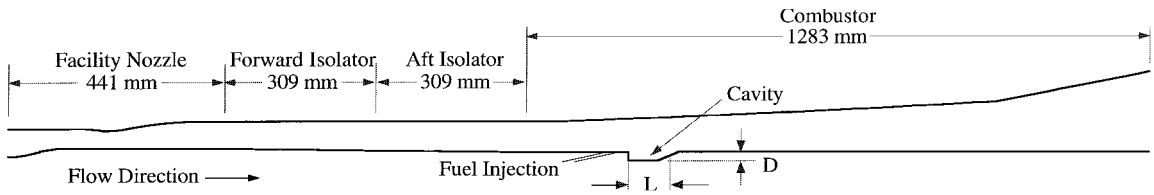

Fig. 1 Flowpath schematic.

Prior to combustion tests, both nozzle–isolator combinations were calibrated to completely document the combustor inlet flowfield at various conditions simulating flight Mach numbers 4, 5, and 6 at dynamic pressures of 47.9 and 95.8 kPa. The calibrations consisted of traversing probe surveys along the vertical centerline of the aft isolator exit using four pitot pressure and two total temperature probes. Furthermore, at each condition, wall static-pressure profiles were acquired at several facility backpressures that were controlled by a butterfly valve. These conditions were also simulated numerically. Experimental and numerical data from these calibrations compare favorably and have been published elsewhere.[36,42–44]

Instrumentation

A CAMAC-based data-acquisition and control system with 416 channels of analog input, 64 channels of digital I/O, and 40 channels of analog output was used. The CAMAC crates were connected to two Sun 630MP workstations via a fiber optic SCSI interface (one each for control and data acquisition). A Pressure Systems Incorporated (PSI) 8400 pressure scanning system consisting of 400 channels with real-time display and data reduction was also used. The facility nozzle had 23 static pressure ports on its side wall. Each isolator had 30 pressure taps on its top and bottom walls (total of 120 taps). The combustor top, bottom, and side walls had more than 1000 static pressure taps; nearly 200 of these taps were instrumented for these tests. A large array of thermocouples was used for monitoring air, fuel, oxygen, cooling-water, and hardware temperatures. These measurements were also used to estimate the heat transfer from the various components. In addition, all flows (air, fuels, water, and oxygen) were measured using either orifice plates or turbine flowmeters.

Remote monitoring of the tests was provided by six video cameras placed throughout the test cell. Four cameras placed around the thrust stand monitored the facility hardware. An infrared camera system provided real-time thermal health monitoring of the heat-sink combustor. Finally, a hand-held Sony 8-mm camera monitored the region near the fuel injector/flameholder through a quartz window. This camera captured visual records of the flame front, flame spreading, and related combustion events.

Results

Combustion tests using the cavity-based fuel injector/flameholder were conducted using two separate facility nozzles (Mach 1.8 and 2.2) to cover a range of combustor conditions simulating flight Mach numbers between 4 and 6 at a flight dynamic pressure of 47.9 kPa. Gaseous ethylene was the combustor fuel for all tests. Wall static pressure data were collected for all tests. Facility parameters such as stagnation pressure and temperature, constituent flow rates (JP-4, ethylene, air, and oxygen), wall temperatures, fuel pressures and temperatures, and load-cell force measurements were recorded as functions of time. Video records of the combustion region near the cavity were obtained. Tables 2 and 3 show the operating conditions, peak pressure rise, and load cell data for tests with the Mach 1.8 and 2.2 facility nozzles, respectively.

Table 2 Operating conditions and results ($M_4 = 1.8$)

Test name	T_{ve},[a] K	P_t, kPa	Peak ϕ	Peak pressure ratio	ΔF, N
98205AC	1001	379.9	0.28	3.11	974
98238AB	1000	379.2	0.45	3.30	1152
98238AC	1001	379.2	0.51	3.39	1228
98238AD	1001	379.9	0.54	3.44	1326
98238AE	1001	379.2	0.60	3.50	1383
98246AG	1000	378.5	0.62	3.57	1472
98260AF	1000	379.2	0.58	——	1379
98260AG	1001	379.2	0.70	3.59	1566
98260AH	1001	380.6	0.75	3.64	1673

[a]Total temperature at combustor inlet is lower than T_{ve} due to heat losses through water-cooled sections.

Table 3 Operating conditions and results ($M_4 = 2.2$)

Test name	T_{ve},[a] K	P_t, kPa	ϕ	Peak pressure ratio	ΔF, N
98323AE	1222	690.9	0.49	3.49	1245
98323AF	1222	691.5	0.55	4.02	1321
98323AH	1223	691.5	0.57	3.86	1423
98342AC[b]	1222	688.8	0.54	3.21	1530
98342AD	1056	692.9	0.50	3.64	1695
98342AE	1000	688.8	0.47	3.93	1779
98342AF	945	689.5	0.31	——	1357
98342AH	1221	690.9	0.53	3.20	1517

[a]Total temperature at combustor inlet is lower than T_{ve} due to heat losses through water-cooled sections.
[b]Aerogrid installed in calorimeter and ethylene preheated to 60°C for test series 98342.

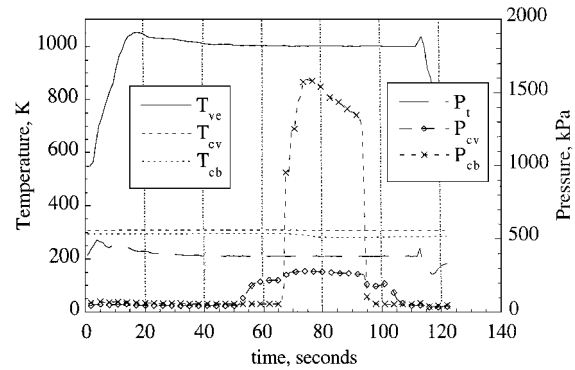

a) Temperature and pressure histories

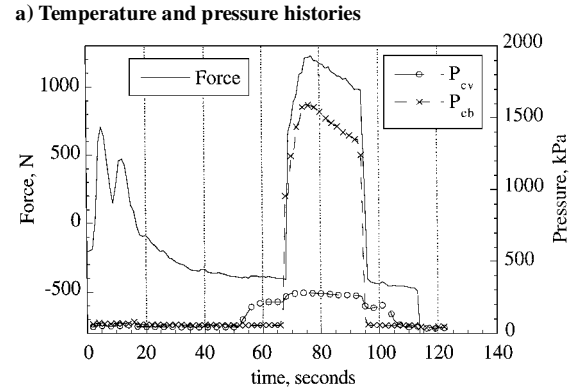

b) Load cell force and fuel pressure histories

Fig. 3 Typical test sequence (test 98260AH).

Sample Test Sequence

Figure 3 provides a sample set of data obtained from test 98260AH that illustrates the sequence of a typical test. Figure 3a shows the time history of three temperatures and three pressures for this test. The temperatures correspond to vitiator exit stagnation temperature T_{ve}, cavity ethylene temperature T_{cv}, and combustor ethylene temperature T_{cb}. The pressure data include facility stagnation pressure P_t, and ethylene supply pressures to the cavity (P_{cv}) and combustor (P_{cb}). Fuel temperatures and pressures were measured inside the respective manifolds immediately upstream of injection. Figure 3b shows the measured load cell force and the fuel pressures on the same time scale. Vitiator ignition occurred around $t = 5$ s, corresponding to the sharp rise in vitiator exit temperature. A large increase in thrust, followed by a gradual decay to steady state, is associated with vitiator ignition (due to the sudden increase in JP-4 flow into the vitiator manifold). The steady-state force measurement has been found to be repeatable to within a few pounds for these conditions. Stable stagnation conditions occur after $t \sim 50$ s.

Once the desired combustor inlet conditions were established, fuel flow was initiated to the cavity, and the cavity manifold pressure increased correspondingly. Shortly after a stable cavity fuel pressure was reached (approximately $t = 15$ s), the spark plugs were

energized, initiating combustion inside the cavity. Combustor main fuel flow was then started. Ignition of the main combustor fuel occurred almost immediately, as indicated by the sudden increase in thrust occurring at $t = 68$ s.

During mainstream combustion, the combustor pressure rise was high enough to feed back into the cavity fuel manifold, resulting in the sudden increase in cavity fuel pressure. Because of the relatively high flow rate and limited supply of ethylene, combustor fuel pressure and temperature both decayed over the course of the test (load cell force decay paralleled the fuel pressure decay), although combustion of the main fuel remained very intense. Combustor fuel flow was terminated at approximately $t = 90$–95 s, after which the load cell force level decreased back to the steady-state value that existed prior to mainstream combustion. The cavity manifold pressure also decreased as the mainstream combustion stopped. Finally, cavity fuel flow was terminated around $t = 105$ s, and the vitiator was extinguished at $t = 110$ s.

Similar test sequencing was used with the Mach 2.2 facility nozzle, except, as noted earlier, the cavity was not fueled independently. Instead, the main fuel was initiated at a very low flow rate, such that sufficient fuel was entrained into the cavity for ignition. Once the cavity was lit, the main fuel flow rate was ramped up to the desired level for mainstream combustion.

Wall Static Pressure Distributions

Figure 4 shows the wall static pressure distributions from test 98260AH. This figure shows the measured wall pressures from the facility nozzle entrance through the isolators and combustor for a tare condition (facility at test condition but no fuel flow) and for the maximum fuel flow condition for this test. An outline of the flowpath is shown above the pressure traces to provide a spatial frame of reference. The gaps in the pressure distributions occur at the physical joints between the nozzle and fore isolator, between the fore and aft isolators, and between the aft isolator and the combustor. Minor disturbances are apparent in the tare pressure distribution; these correspond to interface shocks between the combustor and aft isolator sections and the recompression shock generated at the aft ramp of the cavity flameholder. Aside from these weak waves, the pressure distribution compares well with results of an isentropic analysis.[42,43] Tare and reacting flow pressure distributions were obtained for all test conditions listed in Table 2 with the exception of test 98260AF. In that test, the fuel supply was gradually reduced and no pressure data are presented. The tare measurements for all cases were nearly identical.

Figure 5 contains the wall static pressure distributions measured for several test cases. For clarity, each set of data includes only measurements from the isolators and the combustor. Pressure data from test 98205AC show the presence of main fuel combustion producing a peak pressure ratio of approximately 3.1 near the cavity location.

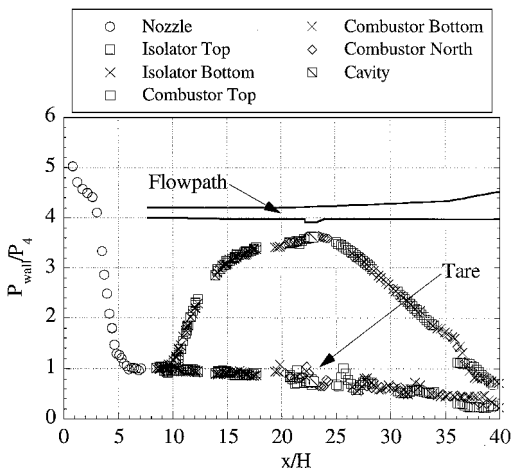

Fig. 4 Normalized tare and reacting flow pressure distributions (test 98260AH, $\phi = 0.75$).

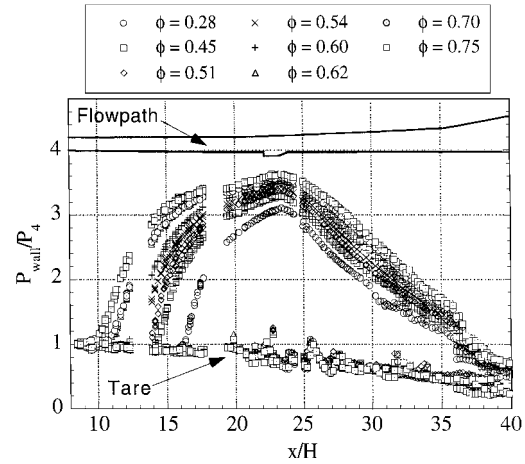

Fig. 5 Isolator/combustor pressure distributions ($M_4 = 1.8$).

For this case, the maximum fuel–air equivalence ratio is about 0.28, and the shock train generated as a result of the combustion-induced pressure rise begins just upstream of the combustor entrance. This case represents the limit of engine operation without appreciable isolator length requirement. As the fuel flow is increased, the normalized pressures increase throughout the isolators and combustor. The shock system moves progressively forward until it is located just downstream of the facility nozzle exit in test 98260AH. At this condition, the maximum equivalence ratio is approximately 0.75, and the corresponding peak pressure ratio is slightly over 3.6. This is representative of a normal shock pressure rise at the conditions entering the combustor. Further increases in fuel flow rate would cause the shock train to move into the facility nozzle section.

With the Mach 2.2 facility nozzle, tare and reacting flow pressure distributions were obtained at all test conditions listed in Table 3 with the exception of test 98342AF. In each case, the tare measurements were nearly identical, suggesting that no appreciable degradation or change occurred in the hardware. Figure 6a includes the 98323 series of tests that were conducted without an aerogrid. Tests from series 98342 were performed with the aerogrid installed in the calorimeter, and are presented in Fig. 6b. The effect of the aerogrid on the combustor exit pressure is clearly evident when the tare pressure data between Figs. 6a and 6b are compared for $x/H > 35$. Over this portion of the combustor, Fig. 6b shows a separated region resulting from the aerogrid blockage. Upstream of the $x/H = 35$ location, the tare pressure traces in Figs. 6a and 6b are nearly identical. The aerogrid has since been modified to decrease the blockage and reduce the influence on the combustor exit flowfield.

Figure 6a shows an increase in peak pressure ratio with increasing equivalence ratio, and a corresponding upstream displacement of the start of pressure rise. With the highest fueling rate used in the present experiments, the start of pressure rise reaches the interface between the two isolators. Experiments with higher fueling rates were not possible due to excessive heat loads that already limited the test runs to about 5 s after initiation of mainstream combustion. The expected trend of increased peak pressure with lower facility stagnation temperature (for approximately the same equivalence ratio) is observed in Fig. 6b. Successful ignition and sustained combustion at the lower stagnation temperatures was achieved by preheating ethylene to 60°C prior to injection. With room-temperature ethylene (test series 98323), ignition and combustion did not occur at facility stagnation temperatures below 1222 K.

Load Cell Force Measurements

Load cell force measurements for the Mach 1.8 facility nozzle experiments appear in Fig. 7a as a function of equivalence ratio. The ΔF values were obtained by subtracting the steady-state force measured prior to combustion from the force measured during combustion. A range of equivalence ratios existed for each test because the fuel pressure was not constant, as indicated by the legend in

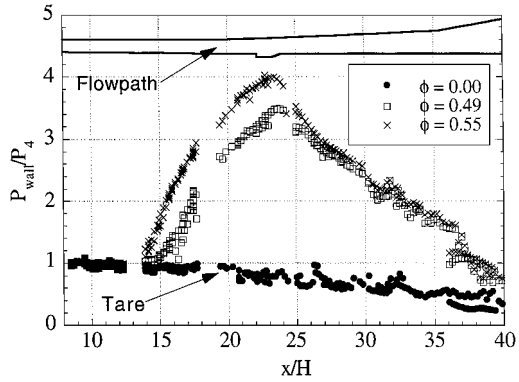

a) No aerogrid, T_t = 1222 K

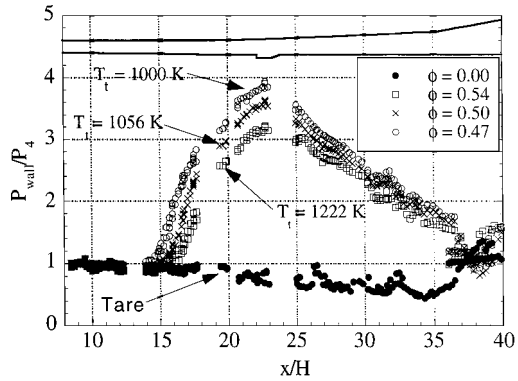

b) With aerogrid

Fig. 6 Isolator/combustor pressure distributions (M_4 = 2.2).

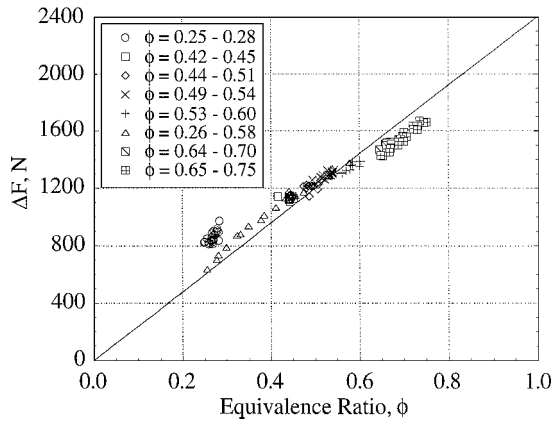

a) M_4 = 1.8

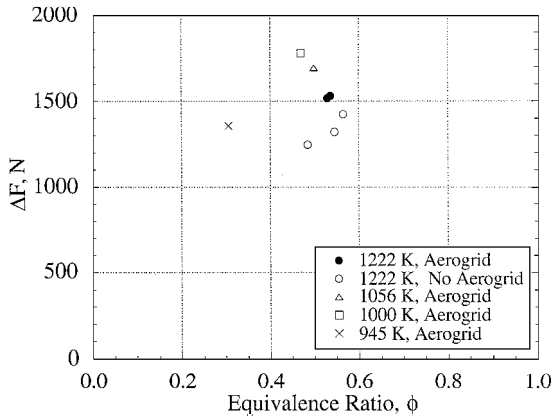

b) M_4 = 2.2

Fig. 7 Variation of ΔF with equivalence ratio.

Fig. 7a. The data show a remarkably linear relationship over the range of equivalence ratios studied. At the higher equivalence ratios ($\phi > 0.6$), the slope of ΔF decreases (relative to the best-fit line), possibly due to decreasing combustion efficiency.

ΔF data with the Mach 2.2 facility nozzle are shown in Fig. 7b. For the three cases at 1222 K without an aerogrid, the relationship is approximately linear, similar to that observed with the Mach 1.8 facility nozzle. For the cases with an aerogrid, higher base pressure on the combustor is the most likely cause of the increase in the load cell force measurement (see Fig. 6b). Pressure instrumentation has been added to the base area of the combustor, and, as discussed earlier, the effects of the aerogrid on thrust and pressure measurements are currently being assessed. The increase in ΔF with decreasing facility temperature is consistent with the rise in peak pressures seen in Fig. 6b. With the Mach 2.2 facility nozzle, the short run durations (unavoidable due to the high heat loads) and the highly unsteady nature of the combustion introduce a larger degree of uncertainty in the average ΔF determined from experimental data.

Reaction Zone Images

Images of cavity combustion and mainstream combustion obtained from the video records of several tests with the Mach 1.8 facility nozzle are presented in Fig. 8. Although these photographs are affected by the limitations inherent in video images (pixel saturation, time-averaging, and line-of-sight integration), they do provide qualitative information about the overall flowfield features. The flow direction is from left to right, and the window is approximately 178 mm long. The leading edge of the cavity is visible in all images. From these photographs, it is evident that the cavity functions well as a flameholder/stabilizer. The flame front observed in these photographs appears anchored at the leading edge of the cavity. Some of the video records, such as Fig. 8d, suggest instability associated with the flame front leading edge and occasional combustion forward of the cavity. Close examination of the video footage reveals that the flame excursions forward of the cavity are localized at the combustor side walls and not in the core region.

A noteworthy observation from the video records is the rate at which the flame appears to spread across the height of the combustor duct. Average flame-spreading angles between 24 and 30 deg are measured. Equivalence ratio appears to have a minor influence on the flame-spreading angle, although the highest equivalence ratio case displays the largest spreading angle. Predictions of jet penetration from the low-angle injectors suggested that approximately half the duct height would contain fuel.[36] Thus, it appears that some other mechanism, additional to the transverse momentum of the fuel, causes the rapid spreading of these flames. The video records suggest that the blockage caused by the presence of the combustion zone turns the airstream upward and toward the top wall of the combustor. This turning of the airstream would naturally transport fuel further from the wall than the jet transverse momentum alone, and could explain the observed flame spreading. Recent OH planar laser-induced fluorescence (PLIF) measurements in the near-field of the injectors show that the flame-spreading rate is reduced compared with the video images.[45] Although the PLIF images indicate that combustion is most likely to occur along the combustor side wall, static pressure measurements on the cavity floor do not show significant spanwise pressure gradients. Although it is speculated that shock/boundary-layer interactions and wall corner effects are among the factors influencing the combustion process, our understanding of the combustion process and its underlying mechanisms is still incomplete and warrants further investigation.

Figure 9 presents similar images obtained from the video records of test 98323AF with the Mach 2.2 facility nozzle. These include a typical image of cavity combustion (low fueling rate through the main injectors), followed by images of main combustion. The leading edge of the cavity is again clearly observed in Figs. 9a, 9b, and 9d. The flame front observed in these photographs is normally anchored at the leading edge of the cavity. The image-to-image variation between Figs. 9b, 9c, and 9d is indicative of instability associated with the flame front.

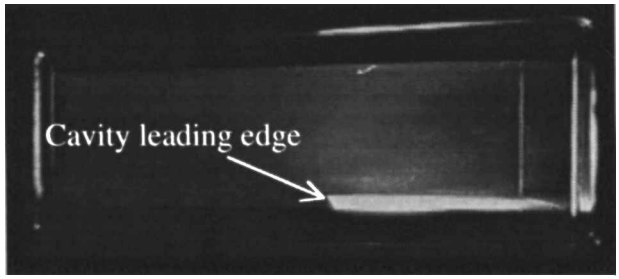

a) Typical image, cavity fuel only

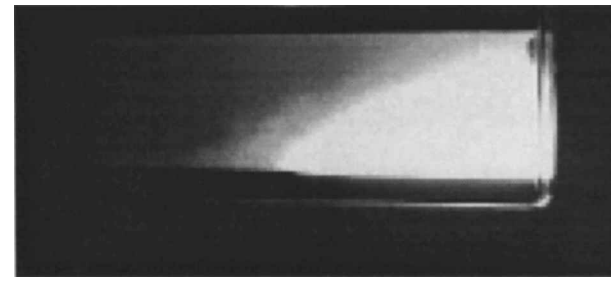

d) Cavity and main fuel, ϕ = 0.49–0.54

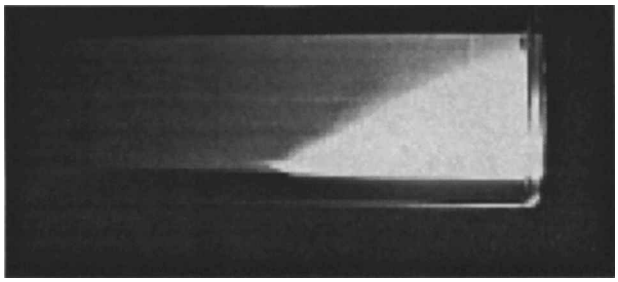

b) Cavity and main fuel, ϕ = 0.42–0.45

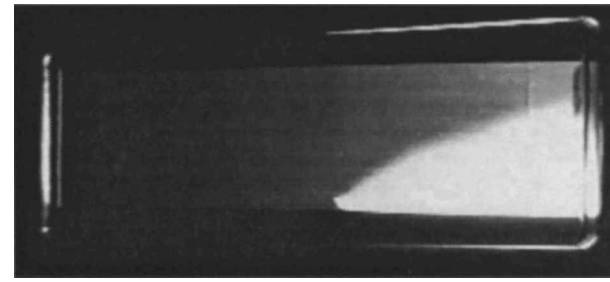

e) Cavity and main fuel, ϕ = 0.64–0.70

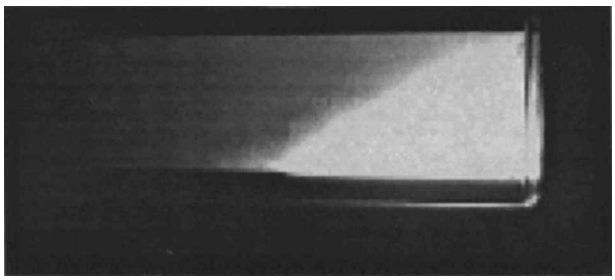

c) Cavity and main fuel, ϕ = 0.44–0.51

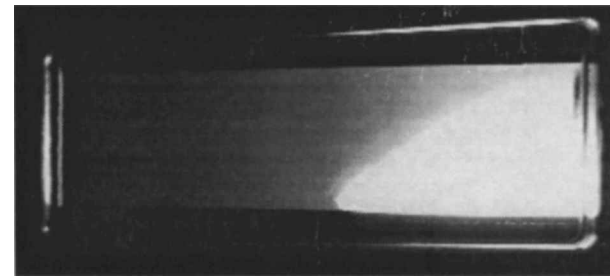

f) Cavity and main fuel, ϕ = 0.65–0.75

Fig. 8 Side view images of flame zones (M_4 = 1.8).

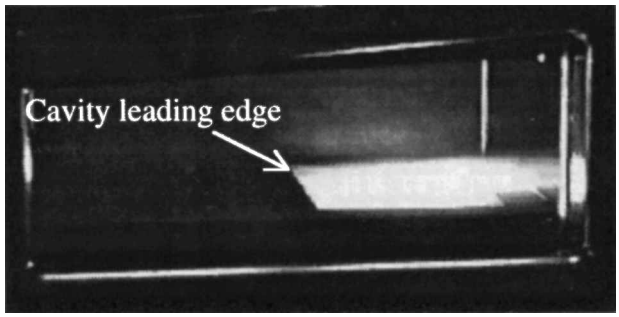

a) Low ϕ, only cavity lit

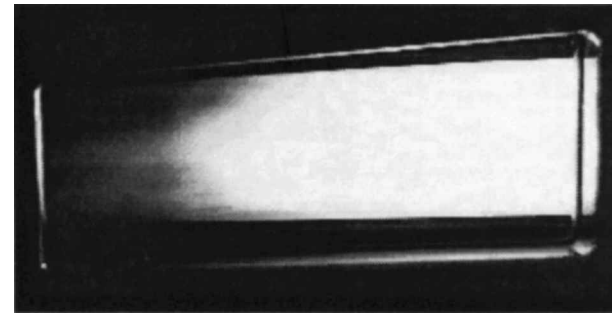

c) Mainstream combustion, ϕ = 0.55

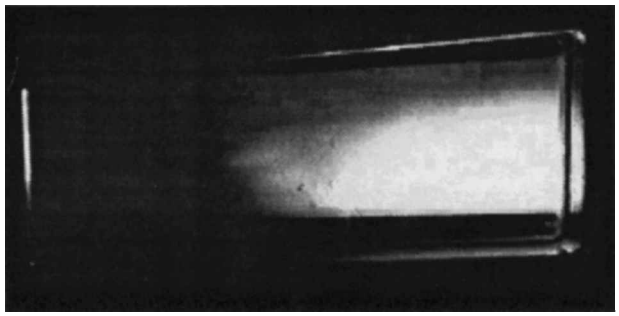

b) Mainstream combustion, ϕ = 0.55

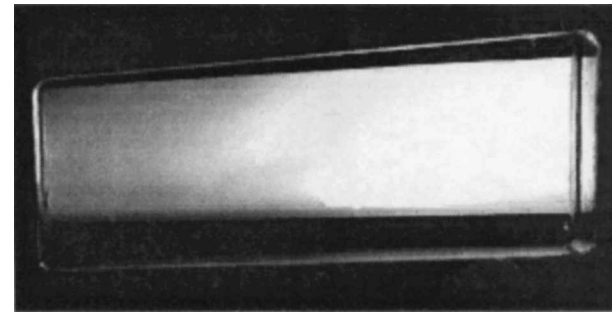

d) Mainstream combustion, ϕ = 0.55

Fig. 9 Side view images of flame zones (M_4 = 2.2, case 98323AF).

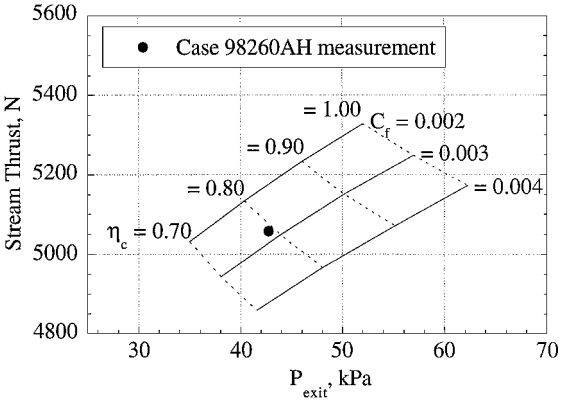

Fig. 10 RJPA analysis (M_4 = 1.8).

Performance Analysis

Combustor performance is assessed using the RJPA code.[46,47] This tool employs a one-dimensional integral simulation for predicting and assessing engine performance. Test data input into the program include combustor geometry, flow rates, temperatures, pressures, and heat fluxes. Combustion efficiency and skin-friction coefficient are parametrically varied to generate a performance map or carpet plot of the particular test (Fig. 10). The ordinate and abscissa represent directly observable quantities. From the measured thrust and exit static pressure, deduced values of combustion efficiency and skin-friction coefficient are 80% and 0.0028, respectively, for test 98260AH with the Mach 1.8 facility nozzle.

Various uncertainties are still being addressed, including more accurate estimates of the transient energy loss into the heat-sink combustor and measurements of combustor base pressure. A sensitivity analysis shows that a 50% change in the combustor heat loss results in only a 5% change in combustion efficiency and no change in the skin-friction coefficient. Further refinements to the analysis and instrumentation capabilities are currently underway. Additionally, future data reduction will also include steam calorimetry as a second, independent assessment of combustion efficiency. Closure with these two techniques will provide confidence in both the facility instrumentation and the estimates for combustor performance.

Summary

A cavity-based flameholder with low-angle flush wall fuel injection upstream of the cavity was successfully demonstrated in a model scramjet combustor using gaseous ethylene. Two facility nozzles were used to simulate combustor inlet flow properties appropriate for flight Mach numbers between 4 and 6 at a dynamic pressure of 47.9 kPa.

1) Combustor operation was sensitive to fuel temperature. The operational envelope expanded to lower facility stagnation temperatures with heated fuel.

2) Ignition and mainstream combustion were achieved at all test conditions reported in this paper using only conventional spark plugs; no other external ignition aids were required.

3) Ignition and combustion produced a precombustion shock train, resulting in dual-mode combustor operation. The shock train became stronger and the starting location of the shock train moved progressively upstream with increasing fuel–air equivalence ratio.

4) Video records showed a very intense combustion zone with rapid flame spreading. On further inspection, it is believed that the observed rapid flame spreading is confined near the sidewalls of the combustor.

5) The cavity-based flameholder concept proved very effective over a wide range of operating conditions and combustor fuel–air equivalence ratios. Over the range of equivalence ratios between 0.25 and 0.75, combustor pressure ratios and delta-force levels were measured between 3.1–4.0 and 667–1779 N, respectively. The delta-force measurements from the Mach 1.8 facility nozzle tests varied nearly linear with equivalence ratio. Preliminary analyses of the experimental results from one test case using the RJPA code yielded an estimate of combustion efficiency near 80% with a corresponding skin-friction coefficient of 0.0028.

Acknowledgments

The U.S. Air Force Hypersonic Technology Program, under the guidance of R. Mercier, provided the funds that made this work possible. The authors acknowledge the contributions of J. Bryant, M. Cox, W. Haendiges, C. Smith, and G. Streby for their technical support. The support of the Research Air Facility at the U.S. Air Force Research Laboratory's Propulsion Directorate is also appreciated.

References

[1]Baurle, R. A., and Gruber, M. R., "Study of Recessed Cavity Flowfields for Supersonic Combustion Applications," AIAA Paper 98-0938, Jan. 1998.

[2]Ben-Yakar, A., and Hanson, R., "Cavity Flameholders for Ignition and Flame Stabilization in Scramjets: Review and Experimental Study," AIAA Paper 98-3122, July 1998.

[3]Davis, D. L., "Numerical Analysis of Two and Three Dimensional Recessed Flame Holders for Scramjet Applications," Ph.D. Dissertation, Aeronautics and Astronautics Dept., Air Force Inst. of Technology, Wright–Patterson AFB, OH, Sept. 1996.

[4]Baysal, O., and Stallings, R. L., "Computational and Experimental Investigation of Cavity Flowfields," *AIAA Journal*, Vol. 26, No. 1, 1988, pp. 6–7.

[5]Chokani, N., and Kim, I., "Suppression of Pressure Oscillations in an Open Cavity by Passive Pneumatic Control," AIAA Paper 91-1729, June 1991.

[6]Clark, R. L., Kaufmann, L. G., and Maciulaitis, A., "Aeroacoustic Measurements for Mach 0.6 to 3.0 Flows Past Rectangular Cavities," AIAA Paper 80-0036, Jan. 1980.

[7]Edwards, J. A., and Zhang, X., "Some Aspects of Supersonic Flow over a Cavity," AIAA Paper 86-2025, Aug. 1986.

[8]Franke, M. E., and Carr, D. L., "Effect of Geometry on Open Cavity Flow-Induced Pressure Oscillations," AIAA Paper 75-492, March 1975.

[9]Hankey, W. L., and Shang, J. S., "Analyses of Pressure Oscillations in an Open Cavity," *AIAA Journal*, Vol. 18, No. 8, 1980, pp. 892–898.

[10]Jeng, Y. N., and Payne, U. J., "Numerical Study of a Supersonic Open Cavity Flow and Pressure Oscillation Control," *Journal of Aircraft*, Vol. 32, No. 2, 1995, pp. 363–369.

[11]Kim, I., and Chokani, N., "Navier–Stokes Study of Supersonic Cavity Flowfield with Passive Control," *Journal of Aircraft*, Vol. 29, No. 2, 1992, pp. 217–223.

[12]Komerath, N. M., Ahuja, K. K., and Chambers, F. W., "Prediction and Measurement of Flows over Cavities—A Survey," AIAA Paper 87-0166, Jan. 1987.

[13]McGregor, O. W., and White, R. A., "Drag of Rectangular Cavities in Supersonic and Transonic Flow Including the Effects of Cavity Resonance," *AIAA Journal*, Vol. 4, No. 11, 1970, pp. 1959–1964.

[14]Morgenstern, A., and Chokani, N., "Hypersonic Flow Past Open Cavities," *AIAA Journal*, Vol. 32, No. 12, 1994, pp. 2387–2393.

[15]Perng, S. W., and Dolling, D. S., "Passive Control of Pressure Oscillations in Hypersonic Cavity Flow," AIAA Paper 96-0444, Jan. 1996.

[16]Rizzetta, D. P., "Numerical Simulation of Supersonic Flow over a Three-Dimensional Cavity," *AIAA Journal*, Vol. 26, No. 7, 1988, pp. 799–807.

[17]Rockwell, D., and Naudascher, E., "Review—Self-Sustaining Oscillations of Flow Past Cavities," *Journal of Fluids Engineering*, Vol. 100, No. 6, 1978, pp. 152–165.

[18]Sarno, R. L., and Franke, M. E., "Suppression of Flow-Induced Pressure Oscillations in Cavities," *Journal of Aircraft*, Vol. 31, No. 1, 1994, pp. 90–96.

[19]Vakili, A. D., Wolfe, R., Nagle, T., and Lambert, E., "Active Control of Cavity Aeroacoustics in High Speed Flows," AIAA Paper 95-0678, Jan. 1995.

[20]Zhang, X., and Edwards, J. A., "Computational Analysis of Unsteady Supersonic Cavity Flows Driven by Thick Shear Layers," *Aeronautical Journal*, Vol. 92, No. 919, 1988, pp. 365–374.

[21]Zhang, X., and Edwards, J. A., "An Investigation of Supersonic Oscillatory Cavity Flows Driven by Thick Shear Layers," *Aeronautical Journal*, Vol. 94, No. 940, 1990, pp. 355–364.

[22]Zhang, X., and Edwards, J. A., "Experimental Investigation of Supersonic Flow over Two Cavities in Tandem," *AIAA Journal*, Vol. 30, No. 5, 1992, pp. 1182–1190.

[23]Zhang, X., and Edwards, J. A., "Computational Analysis of Supersonic Jet and Instability Wave Interaction," AIAA Paper 94-2194, June 1994.

[24]Zhang, X., "Compressible Cavity Flow Oscillation due to Shear Layer Instabilities and Pressure Feedback," *AIAA Journal*, Vol. 33, No. 8, 1995, pp. 1404–1411.

[25]Huellmantel, L. W., Ziemer, R. W., and Cambel, A. B., "Stabilization of

Premixed Propane–Air Flames in Recessed Ducts," *ARS Journal*, Jan. 1957, pp. 31–43.

[26]Hsu, K.-Y., Goss, L. P., and Roquemore, W. M., "Characteristics of a Trapped-Vortex Combustor," *Journal of Propulsion and Power*, Vol. 14, No. 1, 1998, pp. 57–65.

[27]Katta, V. R., and Roquemore, W. M., "Study on Trapped-Vortex Combustor—Effect of Injection on Flow Dynamics," *Journal of Propulsion and Power*, Vol. 14, No. 3, 1998, pp. 273–281.

[28]Niioka, T., Terada, K., Kobayashi, H., and Hasegawa, S., "Flame Stabilization Characteristics of Strut Divided into Two Parts in Supersonic Airflow," *Journal of Propulsion and Power*, Vol. 11, No. 1, 1995, pp. 112–116.

[29]Yu, K., Wilson, K. J., Smith, R. A., and Schadow, K. C., "Experimental Investigation on Dual-Purpose Cavity in Supersonic Reacting Flows," AIAA Paper 98-0723, Jan. 1998.

[30]Vinogradov, V., Grachev, V., Petrov, M., and Sheechman, J., "Experimental Investigation of 2-D Dual Mode Scramjet with Hydrogen Fuel at Mach 4–6," AIAA Paper 90-5269, Oct. 1990.

[31]Vinogradov, V., Kobigsky, S., and Petrov, M., "Experimental Investigation of Liquid Carbonhydrogen Fuel Combustion in Channel at Supersonic Velocities," AIAA Paper 92-3426, July 1992.

[32]Vinogradov, V. A., Kobigsky, S. A., and Petrov, M. D., "Experimental Investigation of Kerosene Fuel Combustion in Supersonic Flow," *Journal of Propulsion and Power*, Vol. 11, No. 1, 1995, pp. 130–134.

[33]Romankov, O. N., and Starostin, F. I., "Design and Investigation of the Stand and Flying Scramjet Models Conceptions and Results of Experiments," AIAA Paper 93-2447, June 1993.

[34]McClinton, C., Roudakov, A., Semenov, V., and Kopehenov, V., "Comparative Flow Path Analysis and Design Assessment of an Axisymmetric Hydrogen Fueled Scramjet Flight-Test Engine at a Mach Number of 6.5," AIAA Paper 96-4571, Nov. 1996.

[35]Mathur, T., Streby, G., Gruber, M., Jackson, K., Donbar, J., Donaldson, W., Jackson, T., Smith, C., and Billig, F., "Supersonic Combustion Experiments with a Cavity-Based Fuel Injector," AIAA Paper 99-2102, June 1999.

[36]Baurle, R. A., Mathur, T., Gruber, M. R., and Jackson, K. R., "Numerical and Experimental Investigation of a Scramjet Combustor for Hypersonic Missile Applications," AIAA Paper 98-3121, July 1998.

[37]Hsu, K.-Y., Carter, C., Crafton, J., Gruber, M., Donbar, J., Mathur, T., Schommer, D., and Terry, W., "Fuel Distribution about a Cavity Flameholder in Supersonic Flow," AIAA Paper 2000-3583, July 2000.

[38]Gruber, M. R., Baurle, R.A., Mathur, T., and Hsu, K.-Y., "Fundamental Studies of Cavity-Based Flameholder Concepts for Supersonic Combustors," *Journal of Propulsion and Power*, Vol. 17, No. 1, 2001, pp. 146–153.

[39]Eklund, D. R., and Gruber, M. R., "Study of a Supersonic Combustor Employing an Aerodynamic Ramp Pilot Injector," AIAA Paper 99-2249, June 1999.

[40]Eklund, D. R., Baurle, R. A., and Gruber, M. R., "Numerical Study of a Scramjet Combustor Fueled by an Aerodynamic Ramp Injector in Dual-Mode Combustion," AIAA Paper 2001-0379, Jan. 2001.

[41]Thompson, M. W., "Equilibrium Chemistry Steam Calorimetry Data Analysis Procedure Using the Ramjet Performance Analysis Code," Rept. RTDC-TPS-028, Johns Hopkins Univ./Applied Physics Lab., Baltimore, MD, 1997.

[42]Gruber, M., Donbar, J., Jackson, K., Mathur, T., Baurle, R., Eklund, D., Cox-Stouffer, S., and Smith, C., "A Newly Developed Direct-Connect High-Enthalpy Supersonic Combustion Research Facility," *Journal of Propulsion and Power*, Vol. 17, No. 6, 2001, pp. 1296–1304.

[43]Jackson, K., Gruber, M., Mathur, T., Streby, G., Smith, C., and Billig, F., "Calibration of a Newly Developed Direct-Connect High-Enthalpy Supersonic Combustion Research Facility," AIAA Paper 98-1510, April 1998.

[44]Gruber, M., Jackson, K., Mathur, T., and Billig, F., "Experiments with a Cavity-Based Fuel Injector for Scramjet Applications," International Symposium on Air Breathing Engines, ISABE Paper IS-7154, Sept. 1999.

[45]Donbar, J. M., Gruber, M. R., Jackson, T. A., Carter, C. D., and Mathur, T., "OH PLIF Imaging in a Hydrocarbon-Fueled Scramjet Combustor," *Proceedings of the Combustion Institute*, Vol. 28, 2000, pp. 679–687.

[46]Pandolfini, P. P., Billig, F. S., Corpening, G. P., Corda, S., and Friedman, M. A., "Analyzing Hypersonic Engines Using the Ramjet Performance Analysis Code," *APL Technical Review*, Vol. 2, No. 1, 1990, pp. 68–79.

[47]Pandolfini, P. P., and Friedman, M. A., "Instructions for Using Ramjet Performance Analysis (RJPA)—IBM-PC Version 1.24," Rept. AL-92-P175, Johns Hopkins Univ./Applied Physics Lab., Baltimore, MD, 1992.